Hindawi
Advances in Multimedia
Volume 2021, Article ID 6337431, 6 pages
https://doi.org/10.1155/2021/6337431

Research Article

Multimedia Digital Signal Processing of Infrared Chemical Remote Sensing Based on Piecewise Linear Discriminant Algorithm

Meitao Gong

Jining Normal University, Inner Mongolia, Jining,
Key Laboratory of High Speed Signal Processing and Internet of Things Technology and Application in Jining Normal University, China

Correspondence should be addressed to Meitao Gong; jnsygmt@mail.poe.edu.pl

Received 8 July 2021; Accepted 20 August 2021; Published 20 September 2021

Academic Editor: Zhendong Mu

According to the basic principle of piecewise linear classifier and its application in the field of infrared chemical remote sensing monitoring, the characteristics of unilateral piecewise linear classifier applied to the infrared spectrum identification of chemical agents are studied. With the characteristic of separate transmission, the characteristic recovery with the total observed deviation is used for the model. The relaxation factors are used to replace the constrained conditions that cannot be optimized into constrained separate line segment calculation conditions. Experiments show that the result of signal recovery is better than traditional Wiener filtering and Richardson–Lucy methods.

1. Introduction

Sensors mainly show signals that are fused together with different factors (noise and ineffective signals), and the transmission path is more complicated. Even if a sensor with a higher function is used, the signal results that can be obtained are not ideal. So, it is not easy to obtain the initial signal of a physical characteristic. But deconvolution is a way to feed back the original signal based on the fused signal. This method is widely used in different fields such as communication, radar, voice, and medicine [1–4].

At present, the more advanced technology is the variation recovery method of Chan et al. The partial differential gradient projection method is used to carry out the Lagrangian multiplier items to minimize the difference in the calculation. The advantages are fast convergence, stability, etc., especially suitable for signals with steep edges. For the regular dynamic adaptive calculation method, the calculation of difference value is also carried out. We published a variation model of deformation and constraint [5]. Under this premise, in this article, the restoration of infrared chemical remote sensing multimedia digital signals is proposed based on the boundary variation model, and at the same time, this model is equivalently segmented for calculation and judgment, and the original signal is appropriately restored [6].

2. Piecewise Linear Discriminant Algorithm

A multimedia digital signal processing method for infrared chemical remote sensing is put forward based on piecewise linear discriminant algorithm. The principle is shown in Figure 1, which is divided into two steps:

Step 1: the received signal sequence is segmented by length N, and the energy of each segmented signal sequence $y_j = \sum_{i=1}^{N_1} |x_{jN_1} + i|^2$, $N = N_1 N_2$, is calculated, which will then be used to obtain the likelihood ratio of the sequential test.

Step 2: calculate the test statistic $\Lambda_K = \sum_{j=1}^{K} \lambda_j$, y_j $1 \le K \le N_2$, and compare it with the thresholds A and B and make a judgment. If $B < \Lambda_K < A$ is always true and the decision cannot be made, to ensure that the test results are obtained within the limited sampling signal

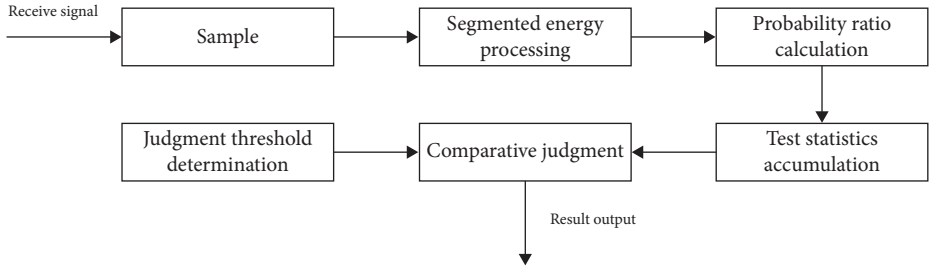

Figure 1: Block diagram of piecewise linear discriminant algorithm processing.

points, piecewise linear discriminant algorithm is used to compare the statistics with the truncation threshold C and make a judgment, namely:

$$\Lambda_{N_2} = \sum_{j=1}^{N_2} \lambda_j \begin{cases} \geq C, & H_1, \\ < C, & H_0. \end{cases} \tag{1}$$

2.1. Likelihood Ratio Calculation. According to the central limit theorem, when the segment length $N1$ is large enough, the segment energy of the received signal y_j approaches the normal distribution process (note: "sufficiently large" usually means that $N1$ must be greater than 0, and the larger $N1$ is, the closer y_j is to the normal distribution process), namely:

$$\begin{aligned} H_0&: y_j \sim \text{Normal}\left(N_1\sigma_w^2, N_1\sigma_w^4\right), \\ H_1&: y_j \sim \text{Normal}\left(\left(N_1 + \frac{\rho}{2}\right)\left(\sigma_w^2 + P\right), \left(N_1 + \rho\right)\left(\sigma_w^2 + P\right)^2\right). \end{aligned} \tag{2}$$

Among them, Normal (μ, σ^2) indicates that it obeys the normal distribution, and then the likelihood ratio expression can be obtained:

$$\begin{aligned} \lambda_j = \ln \frac{f\left(y_i|H_i\right)}{f\left(y_j|H_0\right)} &= \ln\left(\frac{1}{1+\rho}\sqrt{\frac{N_1}{N_1+\rho}}\right) + \frac{\left(y_j - N_1\sigma_w^2\right)^2}{2N_1\sigma_w^4} \\ &- \frac{\left(y_j - \left(N_1 + \rho/2\right)\left(\sigma_w^2 + P\right)\right)^2}{2\left(N_1+\rho\right)\left(\sigma_w^2+P\right)^2}. \end{aligned} \tag{3}$$

Then, the test statistics can be obtained:

$$\Lambda_K = \sum_{j=1}^{K} \lambda_j = K \ln\left(\frac{1}{1+\rho}\sqrt{\frac{N_1}{N_1+\rho}}\right) + \sum_{j=1}^{K}\left[\frac{\left(y_j - N_1\sigma_w^2\right)^2}{2N_1\sigma_w^4} - \frac{\left(y_j - \left(N_1+\rho/2\right)\left(\sigma_w^2+P\right)\right)^2}{2\left(N_1+\rho\right)\left(\sigma_w^2+P\right)^2}\right]. \tag{4}$$

The obtained Λ_K is compared with the thresholds A, B, and C, and a judgment is made; then, the test result can be obtained. According to the central limit theorem, the segmented energy is approximated in the normal distribution process. A very wide probability density distribution function is used for the normal distribution, which not only greatly reduces the computational complexity of the proposed algorithm but also is useful for deriving and analyzing the next spectral perception performance [7].

2.2. Analysis of Average Sample Size. We derive and analyze the average sample size of the proposed algorithm in a complex electromagnetic environment. In this paper, the average sample size of the proposed algorithm in complex electromagnetic environment is deduced and analyze ($\rho \ll 1$) and the likelihood ratio of $N_1 > 10$ is used to calculate the mathematical expectation:

$$\begin{cases} E\left[\lambda_j|H_0\right] \approx -0.5N_1\rho^2 - \rho, \\ E\left[\lambda_j|H_1\right] \approx 0.5N_1\rho^2 + 0.5\rho. \end{cases} \tag{5}$$

By substituting formula (5) into formula (6), the average capacity samples under the dual hypothesis test conditions can be obtained as follows:

$$\begin{cases} \text{ASN}_{H_0} = N_1 E\left(N_2|H_0\right) = -\dfrac{\alpha A + (1-\alpha)B}{0.5\rho^2 + \rho/N_1}, \\ \text{ASN}_{H_1} = N_1 E\left(N_2|H_1\right) = \dfrac{(1-\beta)A + \beta B}{0.5\rho^2 + 0.5\rho/N_1}. \end{cases} \tag{6}$$

According to the above analysis, the average capacity sample ASN, segment length $N1$, and received signal-to-noise ratio of the presented successive inspection algorithm are obtained (ρ). Therefore, in order to obtain the

best detection performance, the functional relationship of the algorithm is discussed in a complex environment, and the detection performance of the proposed algorithm is deduced [8].

Inference 1. In a complex electromagnetic environment ($\rho \ll 1$), in the following cognitive wireless network, the average capacity sample ASN of the piecewise linear determination algorithm based on piecewise energy processing depends on the false alarm probability α and probability of missed detection of the system implemented as needed. In addition, the received signal-to-noise ratio is shown in proportion to the segment length Ni. P is inversely proportional.

Therefore, in order to reduce the average sample size of the proposed algorithm, the segment length $N1$ must be selected as small as possible, but $N1$ needs to meet the central limit theorem condition.

2.3. Discussion on the Best Truncation Threshold. In the successive inspection algorithm, the inequality $B < \Lambda_K < A$ related to the inspection statistics is always established within a certain inspection time, and there is possibility for no judgment. In order to obtain the inspection result within the limited inspection time, finally the inspection statistics are compared with the reduced threshold C to obtain the final judgment result. The threshold C is analyzed for discussion [9].

According to the probability density function of the test statistics shown in Figure 2, the following inequalities describing the false alarm probability and the probability of missed detection of the piecewise linear discriminant algorithm are true:

$$\begin{cases} \alpha(N_2) \le \alpha + \dfrac{\exp B - 1}{\exp B - \exp A} \displaystyle\int_C^A f\left(\Lambda_{N_2} | H_0\right) \mathrm{d}\Lambda_{N_2}, \\ \beta(N_2) \le \beta + \dfrac{\exp B(1 - \exp A)}{\exp B - \exp A} \displaystyle\int_B^C f\left(\Lambda_{N_2} | H_1\right) \mathrm{d}\Lambda_{N_2}. \end{cases} \tag{7}$$

In order to obtain the best detection performance, $\alpha(N_2) + \beta(N_2)$ must be forced to take the minimum value, so C is chosen to minimize the sum of the terms on the right side of the equation, namely:

$$\min G(C) = \frac{\exp B - 1}{\exp B - \exp A} S_0 + \frac{\exp B(1 - \exp A)}{\exp B - \exp A} S_1, \tag{8}$$

where S_0 and S_1, respectively, represent the definite integral term in formula (4). Taking the derivative of formula (8) ($G'(C) = 0$) to solve the equation $f(C|H_0)/f(C|H_1) = \exp B(1 - \exp A)/\exp B - 1$, the optimal truncation threshold under low signal-to-noise ratio ($\rho \ll 1$) can be approximated for:

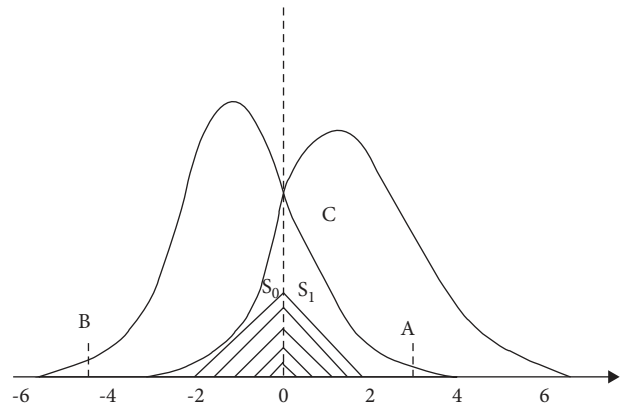

Figure 2: Schematic diagram of the probability density distribution function of the test statistic.

$$C = -0.25 N_2 \rho + (\mathrm{AB} + B) \frac{0.25 - \rho N_1 + \rho^2 \left(N_1 + N_1^2\right)}{N_2 \left(N_1 \rho^2 + 1.5\rho\right)}. \tag{9}$$

Therefore, the sequential inspection algorithm based on the proposed infrared chemical remote sensing multimedia digital signal processing is executed by performing the segmented energy summation processing on the received signal. Sequentially check that the measured likelihood ratio follows the normal distribution process, which greatly simplifies the subsequent calculation and theoretical derivation process. In addition, by introducing the restriction of reduction, it is possible to ensure that the best inspection results can be obtained within a limited inspection time [10–12].

3. Feature Extraction of Frequency-Domain Signals

Fourier transform and expansion are regarded as weighting functions that can be applied to interference graphs used for the Fourier transformation, and the Fourier transformation procedure is usually used to reduce the size of the side lobes. The signal feature extraction technology based on background subtraction technology is only used in fixed-state applications. Therefore, in order to install the sensor to the mobility tool, a new signal feature extraction technology is required, and a time-domain filtering technology is required.

Figure 3 shows the basic principle of time-domain filtering. Theoretically, the time-domain filter can be obtained through the fast Fourier transform of the frequency-domain filter, but in fact, the filtering performance obtained in this way is difficult to meet the requirements. In order to obtain practical time-domain filtering, the spectral data must be filtered in the frequency-domain first, the filtered time-domain data are obtained through fast Fourier transform, and then the time-domain data before and after filtering are used for optimization. The most common finite impulse response (FIR) filter can be expressed as follows:

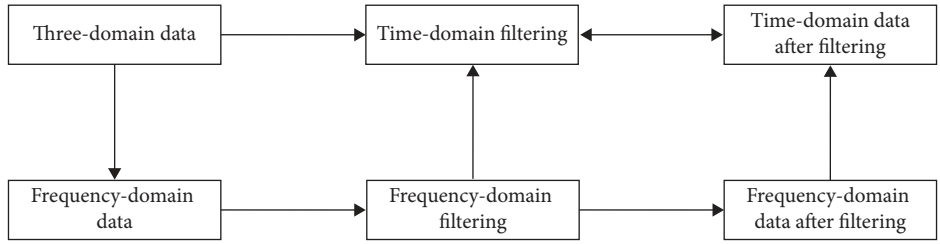

Figure 3: Basic principle of time-domain filter.

$$Y_i^* = f_1 Y_{i-N} + f_2 Y_{i-N+1} + \cdots + f_N Y_{i-1} + f_{N+1} Y_i, \quad (10)$$

where Y_i^* represents filtered data points generated by applying filter; Y_i represents corresponding original data points; and f represents the weighting factor that determines the attribution of the filtering frequency. Each project has different weights of various factors ($f_i \longrightarrow f_{N+1}$).

According to an example method, the well-known variable averaging filter is in the form described above, and each factor is $1/(N+1)$. The linear combination of the corresponding original data points and the previous set of original data points can effectively form filtered data points. Usually, the f term can be solved by multilinear regression analysis. The basic limitation of this filter depends on the filter that handles a relatively wide range of interference graphs. When a filter for each point of the divided interference graph is obtained, the overall accuracy of the filtering process can be improved. Of course, in order to achieve this export process, a large set of interference patterns needs to be used. By performing discrete multiple regressions and checking the filter of each interferogram point separately, one filter coefficient obtained is $(N+1) \times (N+1)$ matrix. This filter is called a finite impulse response matrix (FIRM) filter. Compared with FIR filters, the advantages of FIRM filters are that they can further improve the discrimination rate and the price paid is a smaller application range.

Figure 4 shows the sum of squares of the point intensities of the SF6 interference figure dataset after FIRM filtering. It can be seen from the figure that compared with the baseline fluctuation, the SF6 signal is effectively amplified.

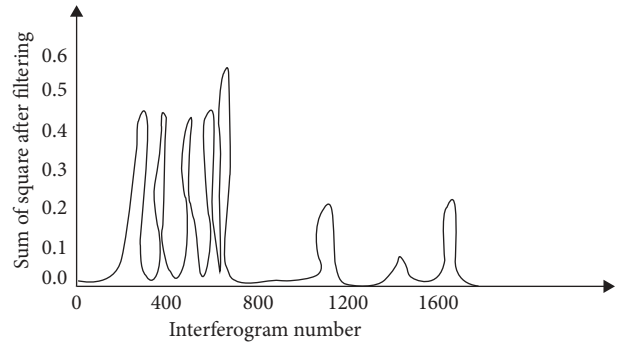

Figure 4: The modulation intensity of the SF6 interference figure dataset in the interval between 175 and 250 after FIRM filtering (the peak value is the SF6 signal, and the baseline is the background signal).

4. Simulation Experiment

In order to verify the effectiveness of the algorithm, the most common step signal is taken in signal transmission as an example, the observation signal is generated from equation (2), and a function suitable for Gaussian distribution is used as the kernel function $h(n)$. For noise with different signal-to-noise ratios (SNRs) added, the Wiener filtering algorithm and the Richardson–Lucy method are used to restore the aforementioned mixed signal with the algorithm proposed in this paper, and the comparison result is shown in Figure 5.

Figures 5(a)–5(c) show the comparison of different algorithms for the recovery effect of multimedia digital signal of infrared chemical remote sensing. In the figure, under the same conditions, the algorithm in this paper is equivalent to the two before the smoothness of the signal is guaranteed to the greatest extent in the smooth section of the signal. More than that, even under the condition of low signal-to-noise ratio, the step position of the restored signal can be clearly seen with the steep edge. This point is important for the sensor signal transmission process, and the jump point usually reflects the potential information of the signal. Under the condition of high signal-to-noise ratio, the observed signal can almost be restored to the original signal [13].

In order to further illustrate the recovery effect of signal, the above results are quantitatively evaluated using the mean square error (MSE) formula in the evaluation standard model of signal restoration quality.

$$\mathrm{MSE} = \sqrt{\sum_{i=1}^{N} \frac{\left(f_i + \widehat{f}_i\right)^2}{N}}. \quad (11)$$

The MSE of the original signal and the recovered signal is calculated, and the results are shown in Table 1 and Figure 6.

The MSE data in Table 1 also show that the restoration effect of the algorithm in this paper is better than the previous two. In the meantime, as the signal-to-noise ratio increases, the MSE before and after restoration will become smaller and smaller.

h_ε and μ in the TBV model are important values that depend on the result. The meaning of formula (2) is a result of combining the random deviation of the restored signal with the observed signal. The result value is obtained. ε reaches the numerical requirement. μ ($\mu > 0$) in $\max|\eta_i| \le \varepsilon$ can have a compromise effect on the fully bounded variation value and the observed error term. If the value of μ is

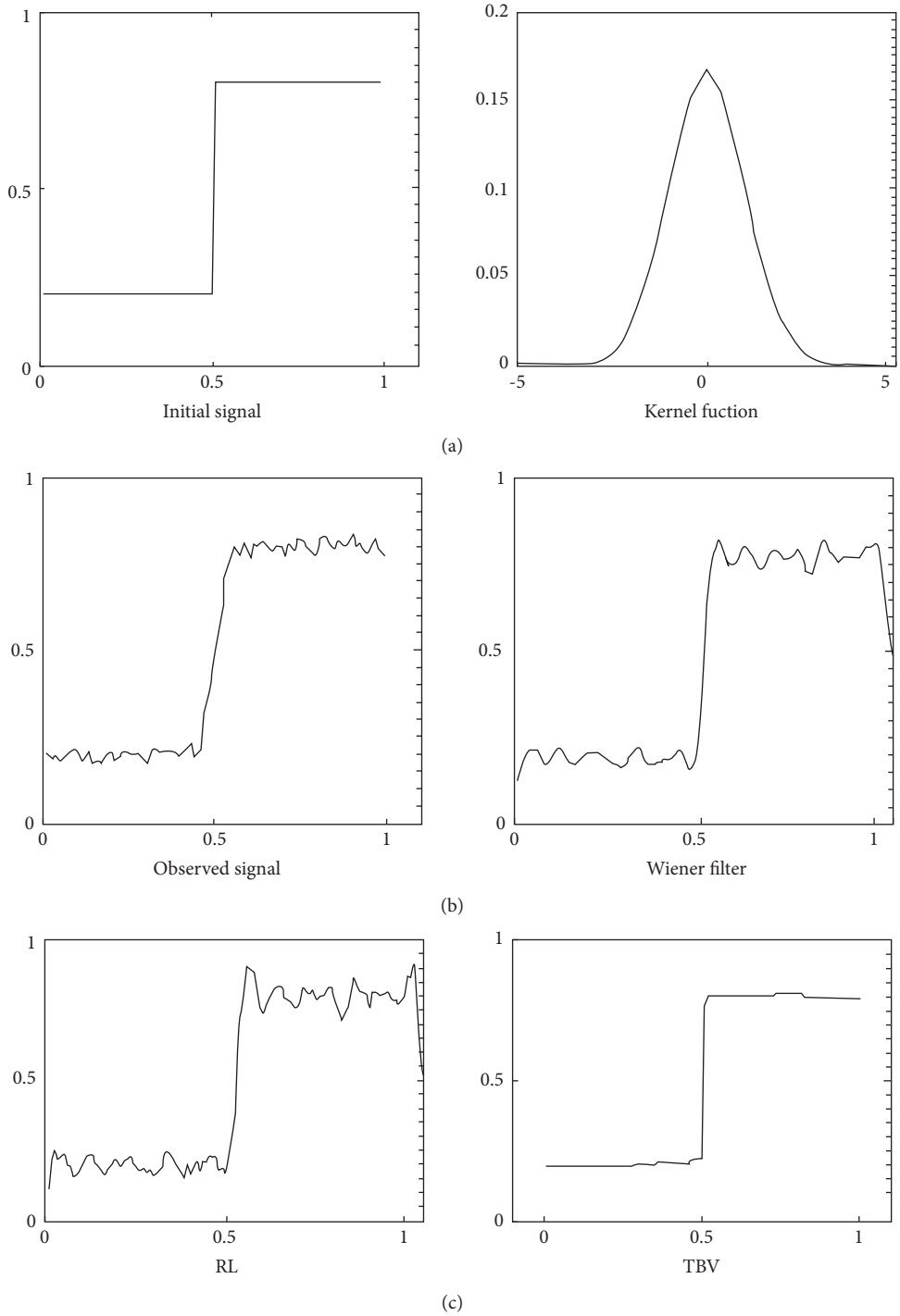

Figure 5: Signal restoration comparison chart: SNR = 30 dB and TBV parameter $\mu = 1$.

Table 1: MSE of the restored signal and the original signal (different algorithms).

Algorithm($\mu = 1$)	SNR = 1 dB	SNR = 5 dB	SNR = 10 dB	SNR = 30 dB	SNR = ∞
Wiener filtering	0.284087	0.171576	0.124115	0.0558268	0.0289276
Richardson–Lucy	0.659045	0.399964	0.269647	0.0592334	0.0526244
TBV	0.104444	0.0846292	0.0592354	0.00422456	$1.48778e-014$

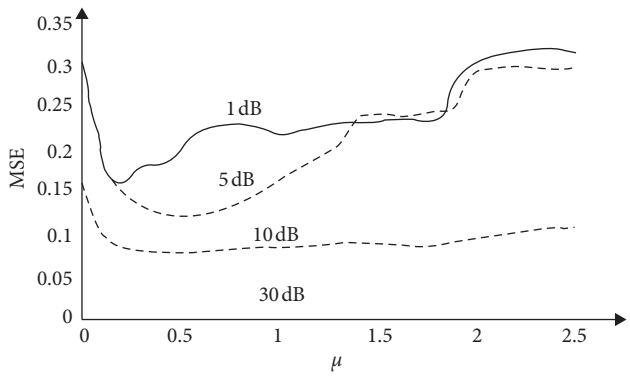

Figure 6: Parameters μ restoration effect under the influence of the signal-to-noise ratio.

large, it will bring a great noise effect; if the value is too small, it will not be able to completely eliminate the blur. Figure 3 shows a variety of signal-to-noise ratios and multiple values. The experimental result achieved by μ is μ-MSE, and most of the values are in a downward convex form, which is to produce the best numerical map under the condition of signal-to-noise ratio. μ represents the minimum value of the original signal and the restored signal. If the value of the signal-to-noise ratio is smaller, if $\mu \in (0, \mu^*)$, the value of μ is larger, and the total observation error will show a decreasing trend. The purpose is to minimize the value of equation (9); simultaneously, if total bounded variation value becomes larger, $\mu = \mu^*$, the MSE obtained is the smallest, which is the most ideal result of restoring the signal; when $\mu \in (\mu^*, \infty)$ increases, the total observation error item is reduced because there must be a stable result state; if the global variation term keeps getting bigger, the MSE will get bigger and bigger, and the signal restoration result will show a downward trend. When the signal noise is larger, the noise in the observation signal becomes smaller. MSE will remain the same [14, 15].

5. Conclusions

Aiming at the smoothness and jump characteristics of infrared chemical remote sensing multimedia digital signal, with regard to the smooth and jumping feature contained by the infrared chemical remote sensing multimedia digital signal. This method can quickly minimize the bounded variation and total observation error and reduce the complexity of the variation parameters. Experiments show that this method is useful and effective, and even in the background of low signal noise, the original signal information can also be restored.

Data Availability

The data used to support the findings of this study are available from the corresponding author upon request.

Conflicts of Interest

The author declares that there are no conflicts of interest.

References

[1] P. C. Guillevic and A. Olioso, S. J. Hook, J. B. Fisher, J.-P. Lagouarde, and E. F. Vermote, "Impact of the revisit of thermal infrared remote sensing observations on evapotranspiration uncertainty—a sensitivity study using ameriflux data," *Remote Sensing*, vol. 13, no. 5, pp. 498–507, 2019.

[2] C. Wu, L. Zhang, and L. Zhang, "A scene change detection framework for multi-temporal very high resolution remote sensing images," *Signal Processing*, vol. 124, pp. 184–197, 2016.

[3] G. Notesco, Y. Ogen, and E. Ben-Dor, "Mineral classification of makhtesh ramon in Israel using hyperspectral longwave infrared (lwir) remote-sensing data," *Remote Sensing*, vol. 7, no. 9, pp. 12282–12296, 2015.

[4] A. Ansari, H. Danyali, and M. S. Helfroush, "Hs remote sensing image restoration using fusion with ms images by em algorithm," *IET Signal Processing*, vol. 11, no. 1, pp. 95–103, 2017.

[5] X. Zhang, "Research on remote sensing image de¨¨aze based on gan," *Journal of Signal Processing Systems*, vol. 73, pp. 620–627, 2021.

[6] F. Bode, W. Nowak, and M. Loschko, "Optimization for early-warning monitoring networks in well catchments should be multi-objective, risk-prioritized and robust against uncertainty," *Transport in Porous Media*, vol. 114, no. 2, pp. 261–281, 2016.

[7] P. Liu, "Development and application of fire safety monitoring and early warning system for small and medium sized hospital enterprises," *Basic and Clinical Pharmacology and Toxicology*, vol. 119, no. Suppl.4, p. 57, 2016.

[8] C. Hua, Y. Tang, M. Ren, and W. Lin, "Single near-infrared fluorescent probe with high- and low-sensitivity sites for sensing different concentration ranges of biological thiols with distinct modes of fluorescence signals," *Chemical Science*, vol. 74, no. 1, pp. 914–923, 2016.

[9] Y.-Z. Liu, Y.-S. Zou, Y.-L. Jiang, H. Yu, and G.-F. Ding, "A novel method for diagnosis of bearing fault using hierarchical multitasks convolutional neural networks," *Shock and Vibration*, vol. 2020, no. 13, 14 pages, Article ID 8846822, 2020.

[10] C. T. Chiang and K. Y. Liu, "A cmos wearable infrared light intensity digital converter for monitoring unplanned self-extubation of patients," *IEEE Sensors Journal*, vol. 14, no. 16, pp. 136–154, 2019.

[11] T. T. de Almeida, J. A. M. Nacif, F. P. Bhering, and J. G. R. Junior, "Doctrams: a decentralized and offline community-based traffic monitoring system," *IEEE Transactions on Intelligent Transportation Systems*, vol. 20, no. 3, pp. 1160–1169, 2019.

[12] B. Cian, M. Suzanne, K. Heard, Q. Peter, S. G. Yeates, and V. Aravind, "Nanoscale infrared identification and mapping of chemical functional groups on graphene," *Carbon*, vol. 139, pp. 317–324, 2018.

[13] V. Singh and M. K. Goyal, "An improved coupled framework for glacier classification: an integration of optical and thermal infrared remote-sensing bands," *International Journal of Remote Sensing*, vol. 101, no. 3, pp. 152–160, 2018.

[14] A. J. Barclay, A. R. W. Mckellar, and N. Moazzen-Ahmadi, "Infrared observation of a new mixed trimer, CO – $(CO_2)_2$," *Chemical Physics Letters*, vol. 677, pp. 127–130, 2017.

[15] L. Hua and G. Shao, "The progress of operational forest fire monitoring with infrared remote sensing," *Journal of Forestry Research*, vol. 228, pp. 71–81, 2017.